Clim Dyn (2015) 45:1789–1799
DOI 10.1007/s00382-014-2433-9

Global radiative adjustment after a collapse of the Atlantic meridional overturning circulation

Sybren S. Drijfhout

Received: 18 August 2014 / Accepted: 29 November 2014 / Published online: 12 December 2014

Abstract The transient climate response to a collapse of the Atlantic meridional overturning circulation (AMOC) is analysed from the difference between two ensembles of climate model simulations with ECHAM5/MPI-OM, one with hosing and the other without hosing. The primary effect of the collapse is to redistribute heat over the two hemispheres. However, Northern Hemisphere sea ice increase in response to the AMOC collapse induces a hemisphere-wide cooling, amplified by atmospheric feedbacks, in particular water vapour. The Southern Hemisphere warming is governed by slower processes. After 25 years the global cooling peaks. Thereafter, the response is characterised by a gradual readjustment of global mean temperature. During the AMOC collapse a downward radiation anomaly arises at the top of the atmosphere (TOA), heating the earth's surface. The net downward radiation anomaly at TOA arises from reduced longwave emission by the atmosphere, overcompensating the increased net upward anomalies in shortwave and longwave radiation at the surface. This radiation anomaly is associated with net ocean heat uptake: cooling of the overlying atmosphere results from reduced ocean heat release through the increase of sea-ice cover in the North Atlantic. The change in energy flow arises from the reduction in latent and sensible heat flux, which dominate the surface radiation budget. Similar experiments with a climate model of intermediate complexity reveal a stronger shortwave response that acts to reduce the net downward radiation anomaly at TOA. The net shortwave and longwave radiation anomalies at TOA always decrease during the first 100 years after the AMOC collapse, but in the intermediate complexity model this is associated with a sign change after 90 years when the net radiation anomaly at TOA becomes upward, accompanied by net ocean heat loss. After several hundred years the longwave and shortwave anomalies increase again, while the net residual at TOA remains small. This radiative adjustment is associated with the transition to a colder climate.

Keywords Thermohaline circulation · Meridional overturning circulation · Abrupt climate change · Atmospheric feedbacks · Bipolar seesaw

1 Introduction

The Atlantic meridional overturning circulation (AMOC) transports large amounts of heat across the equator to the North Atlantic. As a result, it exerts a strong influence on climate in the North Atlantic basin and Northwest Europe (Ganachaud and Wunsch 2003). A shut-down of the AMOC therefore has large climate impacts, with strong cooling in the Northern Hemisphere (NH), in particular over the North Atlantic, and slighter warming in the Southern Hemisphere (SH) (Vellinga and Wood 2002; Drijfhout 2010). The imprint of the AMOC collapse on sea surface temperature (SST) and surface atmospheric temperature (SAT) changes with time. When the freshwater hosing is large enough O(1 $Sv = 10^6$ m^3 s^{-1}), the timescale of the AMOC collapse is about 20 years. This timescale is also associated with the fast atmospheric response to the AMOC collapse (Laurian et al. 2009), which is shaped by sea-ice and snow cover albedo changes, and by water vapour and cloud cover

S. S. Drijfhout
Royal Netherlands Meteorological Institute (KNMI),
PO Box 210, 3730AE De Bilt, The Netherlands

S. S. Drijfhout (✉)
National Oceanography Centre, University of Southampton,
Southampton, UK
e-mail: s.s.drijfhout@soton.ac.uk; drijfhou@knmi.nl

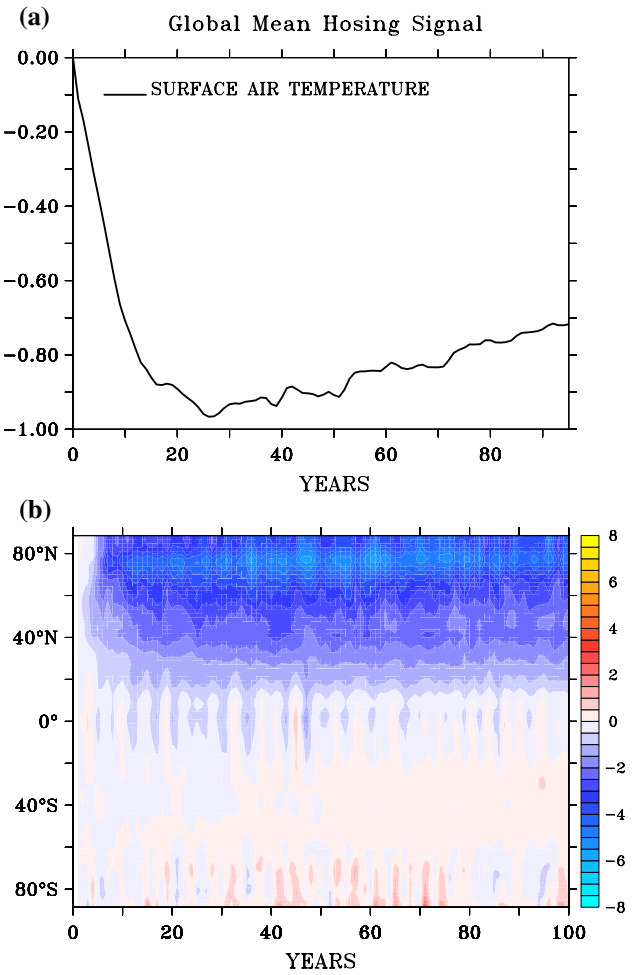

Fig. 1 **a** Trend in GMT after the onset of an AMOC collapse, being the temperature difference between the two ensemble means with and without hosing. Years are counted relative to the start of the freshwater hosing. Values have been smoothed with an 11-year low-pass filter. **b** Zonally averaged surface air temperature response as a function of time, being the different temperature between the two ensemble means

changes (Zhang and Delworth 2005; Cheng et al. 2007; Laurian et al. 2010; Zhang et al. 2010). The water vapour changes are most important in setting the amplitude of the global mean cooling (Laurian et al. 2009), but cloud feedbacks can be significant as well. Without cloud feedback the amplitude of the global cooling was reduced by 30 % in the experiment described in Zhang et al. (2010).

Laurian et al. (2009, 2010) described an experiment in which persistent hosing was combined with increasing CO_2 forcing. Both papers discussed the atmospheric fast response to an AMOC shut down from an equilibrium point of view, that is, like many other papers they defined and investigated a fixed response by comparing averages from two different timeslices. Figure 1a illustrates that in reality the fast atmospheric response is modified by slower processes: the global mean temperature (GMT) anomaly is a function of time. After 25 years from the collapse, the GMT anomaly starts diminishing. The cause of the decline of the GMT anomaly after 25 years has not been discussed before. Here, the mechanisms that cause this decline in GMT anomaly will be investigated in the same experiment discussed in Laurian et al. (2009, 2010), now emphasizing the transient nature of the response. The processes that determine the slow adjustment of the coupled response to an AMOC collapse will be inferred from diagnosing changes in global energy flow (Trenberth et al. 2009). The fast response of O (25 years) and the following, slower response that counteracts the fast response will be interpreted in the framework of the bipolar seesaw (Broecker 1998; Stocker and Johnsen 2003), which recognizes that reduced northward ocean heat transport associated with a collapse of the AMOC causes a dipole anomaly in SST. Evidence for such a dipole pattern has been found in paleodata (Blunier and Brook 2001). Stocker and Johnsen (2003) argued that NH cooling and SH warming feature different timescales arising from the adjustment time of the Southern Ocean heat reservoir. Here, it will be shown that the larger Southern Ocean heat reservoir is associated with slower radiative adjustment in the SH.

2 Experimental set-up

Two five-member ensembles of simulations with the coupled climate model ECHAM5/MPI-OM (Roeckner et al. 2003; Marsland et al. 2003) have been analysed. The ocean component of the climate model has a horizontal resolution of about 1.4°, increasing towards the poles. The meridional resolution is refined near the equator to 0.5°. The ocean model has 40 vertical levels. The atmospheric component has a horizontal resolution of T63 and 31 vertical levels. In both sets of simulations CO_2 concentrations follow the SRES A1b scenario after year 2000 and historical forcing of greenhouse gases and aerosols between years 1950 and 2000. Each ensemble has slightly perturbed initial conditions in year 1950. The second ensemble duplicates the first ensemble until year 2000, after which an AMOC collapse is enforced by permanently adding a freshwater anomaly between 50°N and 70°N in the Atlantic of 1 Sv. This fresh water input is larger than the present-day Greenland ice sheet and clearly not realistic. The AMOC in state-of-the-art coupled climate model, however, is often too stable, Drijfhout et al. (2011), and a 100–150 Sv-year freshwater anomaly is commonly invoked to shut-down the AMOC (Vellinga and Wood 2002; Jackson 2013). All simulations end in the year 2100 when the SRES scenario terminates. To isolate the effect of the AMOC collapse, the difference between the two ensemble means is taken here. Since in

both ensembles exactly the same CO_2 change is prescribed, the difference contains no contribution from changing CO_2. Only when forcing by CO_2 and heat transport change do not add up linearly, the collapse-signal becomes affected by CO_2 changes. Such nonlinearities, however, turn out to be small. The analysis is extended with a hosing experiment in the pre-industrial control run of a coupled climate model of intermediate complexity, SPEEDO (Cimatoribus et al. 2012a).

The Earth system Model of Intermediate Complexity SPEEDO is described in Severijns and Hazeleger (2009). It consists of a coupled atmosphere/land/ocean/sea-ice general circulation model. The atmospheric component of SPEEDO is an atmospheric General Circulation Model, having a horizontal spectral resolution of T30 with a horizontal Gaussian latitude-longitude grid (approximately 3° resolution) and 8 vertical density levels. Simple parameterisations are included for large-scale condensation, convection, radiation, clouds and vertical diffusion. A simple land model is included, with three soil layers and up to two snow layers. The hydrological cycle is represented with the collection of precipitation in the main river basins and outflow in the ocean at specific positions. Freezing and melting of soil moisture is included. The ocean component of SPEEDO has approximately a 3° × 3° resolution in the horizontal, with 20 vertical layers ranging in resolution from 10 to 750 m from the surface to the bottom. The horizontal grid of the ocean model is curvilinear, and deviates from a latitude-longitude grid in the North Atlantic and Arctic basins to avoid the singularity of the north pole. A full complexity sea-ice model is included. A coupler provides the boundary conditions to the components, and performs the interpolations between the different ocean and atmosphere model grids in a conservative way.

The use of SPEEDO allows to infer the longer timescale adjustment by extending the run to 1,200 years. After prolonging the spin-up with 200 years freshwater hosing of 0.5 Sv for 200 years was applied, while freshwater input in the Atlantic was compensated elsewhere in the ocean, demanding no net freshwater addition at each timestep. After year 400, the run was prolonged for 800 years without applying additional freshwater sources.

3 Results

3.1 The fast response in the ECHAM5 ensemble

In response to the hosing the AMOC reduces significantly below a few hundred meters depth, from an annual mean maximum of 22 Sv at 1,000 m depth to a maximum of 3 Sv at 1,500 m depth. Before its collapse the AMOC was associated with a cross-hemispheric heat transport of 0.6 10^{15} W. For each hemisphere, a cessation of this heat transport is equivalent to a radiative forcing at the surface of 2–2.5 W m^{-2}; cooling the NH and warming the SH. Due to this forcing in the NH the temperature quickly drops (Fig. 2a). The change in temperature is associated with a change in upward longwave radiation. This term and all other terms of the surface energy budget (Trenberth et al. 2009) are displayed in Fig. 2b. In the NH, the forcing by diminished heat transport is amplified by reduced longwave back radiation and by increased upward shortwave radiation, related to enhanced reflection by increasing sea-ice (Fig. 2a). The turbulent heat flux, dominated by the latent heat flux changes (less evaporation), and downward shortwave radiation, associated with fewer clouds, especially over land, counteract the forcing, as does the Planck feedback, but the net change in energy flow is amplifying the forcing (Fig. 2b). Changes in longwave radiation dominate the other terms in the surface energy budget; they are induced by water vapour changes and the Planck feedback (Fig. 2a). Once the AMOC has collapsed after 25 years, the heat transport does not alter anymore and fast feedbacks cease to operate. As a result, the various types of energy flow in the NH remain nearly constant (Fig. 2b).

A striking feature is the strong dissimilar response between the NH and SH over the first 100 years (Fig. 1b). The concept of a bipolar seesaw, commonly used to describe the response to an AMOC collapse (Broecker 1998; Stocker and Johnsen 2003), cannot be applied to the fast response during the first 25 years. Initially, temperature changes and atmospheric feedbacks in the SH are much weaker than in the NH (Fig. 2c, a), leaving a net cooling anomaly in GMT. In the NH, the cooling by decreased northward heat transport is quickly amplified by reduced back radiation and by more reflected shortwave radiation (Fig. 2b). In the SH the fast sea-ice albedo feedback is almost absent and the change in back radiation is weak, initially even decreasing, inducing SH cooling instead of warming.

After the AMOC collapses a global radiation imbalance arises that is closed by net global ocean heat uptake (Fig. 2f), heating the global ocean. On top of this global imbalance, there is also a hemispheric radiative imbalance at the air/sea interface heating the NH ocean and cooling the NH atmosphere; and cooling the SH ocean and heating the SH atmosphere. This interhemispheric radiative imbalance must be closed by anomalous southward ocean heat transport across the equator and anomalous northward atmospheric heat transport across the equator. The anomalous southward ocean heat transport arises from the AMOC collapse and is the forcing here. The anomalous northward atmospheric heat transport follows from Bjerknes compensation (Bjerknes 1964) and is a response to the AMOC collapse. Figs. 2a–d consider the energy balance for the

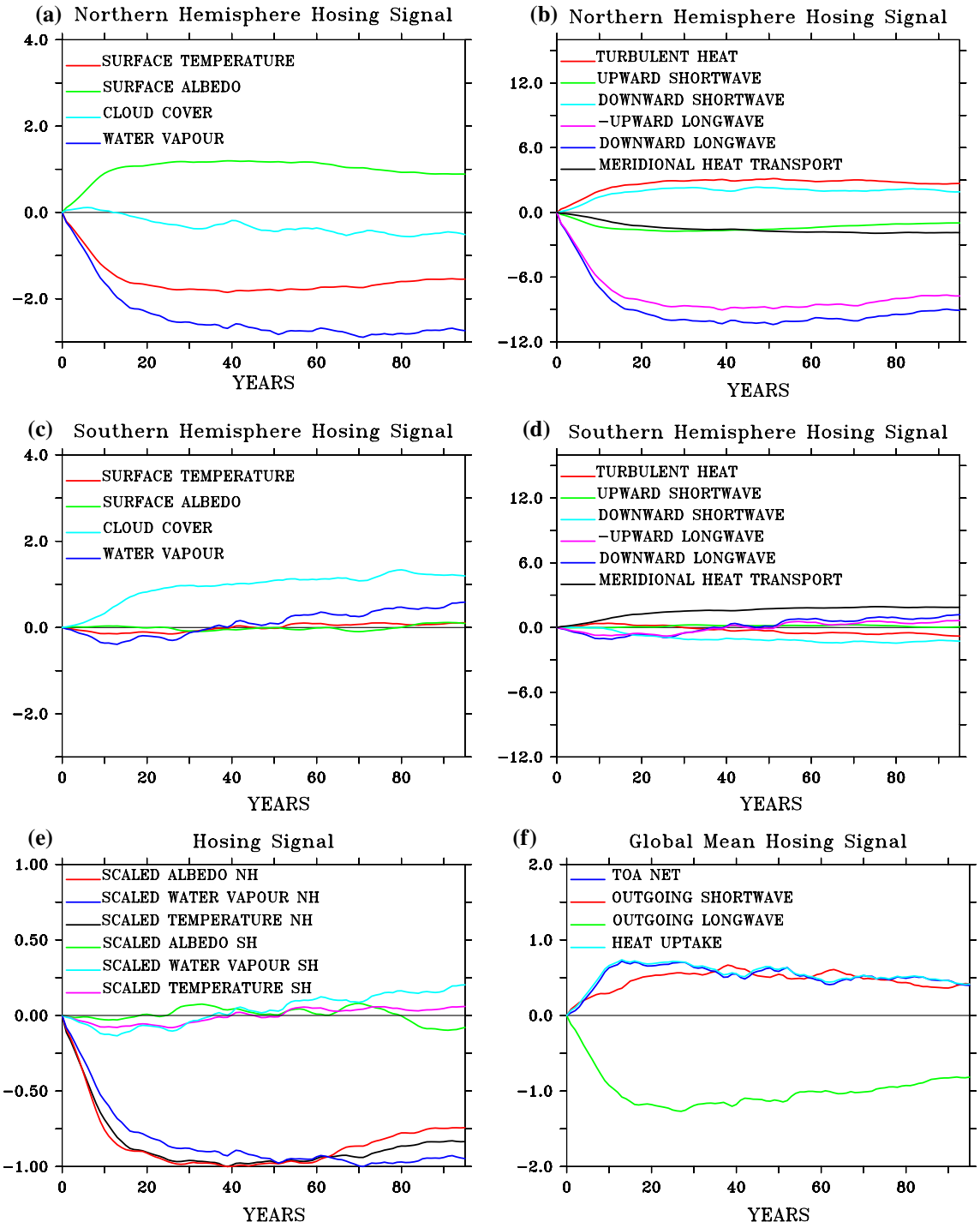

Fig. 2 Trends in energy flow in W m^{-2} and in 4 climate parameters. All values have been smoothed with an 11-year low-pass filter. **a** Difference between the two ensemble means in NH temperature in °C; albedo; cloud cover in percentage; and water vapour content in kg m^{-2}. **b** Difference between the two ensemble means in NH energy flow. **c** Same as **a**, but for the SH. **d** Same as **b**, but for the SH. **e**) Nondimensional variation in difference between the two ensemble means for three climate parameters scaled by their NH extreme. **f** Difference between the two ensemble means in globally averaged TOA radiation and ocean heat uptake

ocean only; a similar diagram could have been drawn for the atmosphere, but with reverse signs. In both ocean and atmosphere net cooling in the NH arises because the sum of heat transport anomaly; net shortwave, downward longwave and turbulent heat loss anomalies do not close. They require a large reduction in upward longwave radiation

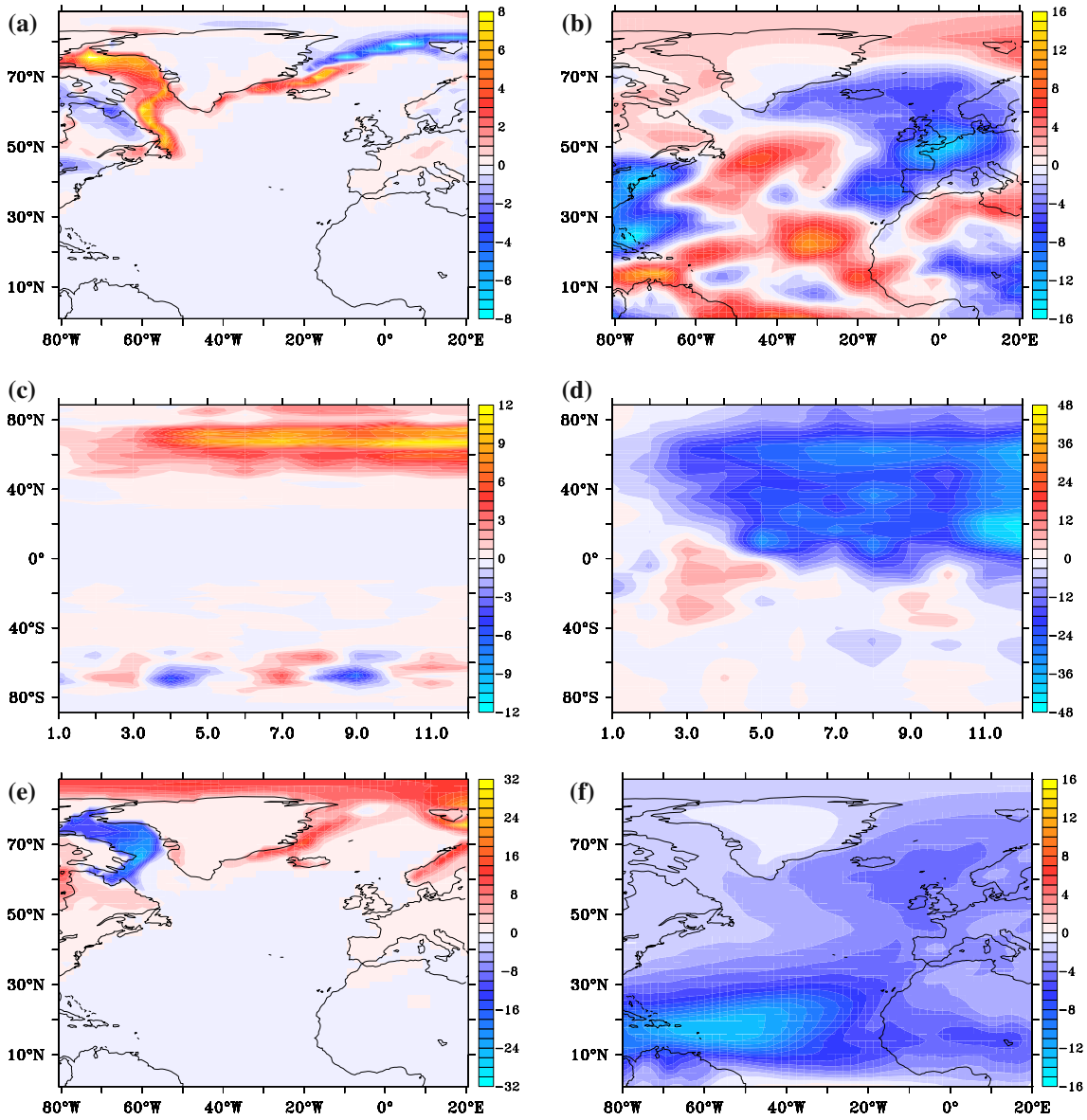

Fig. 3 Water vapour content and albedo anomalies associated with the AMOC collapse. **a** Yearly-averaged albedo anomaly at year 1 in percentage. **b** Yearly-averaged water vapour content anomaly at year 1 in 100 g m^{-2}. **c** Hövmoller diagram of yearly-averaged albedo anomaly in percentage averaged between 80°W and 0°W, as a function of latitude and time for years 1–12. **d** Same for water vapour content in 100 g m^{-2}, but zonally averaged between 40°W and 20°E. **e** Ten-year averaged albedo anomaly for years 90–100. **f** Ten-year averaged water vapour content anomaly for years 90–100 in kg m^{-2}

arising from cooler surface temperatures. In the SH such a radiation imbalance at the air/sea interface initially does not occur, despite a similar forcing (but reversed in sign) from anomalous heat transport. As a result, the net warming in the SH is much smaller. The key to this different behaviour between the two hemispheres is the sea-ice response. The response to a prescribed sea-ice change in both hemispheres is similar (Chiang and Bitz 2005). The sea-ice response to a change in the AMOC, however, is highly dissimilar (Fig. 2a, c), see also Stouffer et al. (2006). During the collapse of the AMOC, sea-ice changes in the NH lead the water vapour changes (Fig. 2e). Also, NH water vapour anomalies arise first downstream of areas where sea-ice increases and inhibits evaporation (Fig. 3a, b).

Sea-ice starts increasing in the western Labrador Sea, off the Canadian coast. Locally, the atmosphere cools due to capping of the ocean by sea-ice and the cooler atmosphere must reduce its water vapour content even further because of the Clausius–Clapeyron equation. The water vapour anomaly is transported eastward by westerly winds and reaches maximum amplitude in the eastern North Atlantic and west European continent at the same latitude of the

sea-ice anomaly (Fig. 3b). The drying initiated by sea-ice increase is amplified by atmospheric cooling. Thereafter, the negative water vapour anomalies progress further southward by transport and mixing, while the sea-ice anomaly remains within the latitude band between 50°N and 70°N. (Fig. 3c, d). Also, the wind-evaporation-SST feedback plays a role in the southward progress of the water vapour anomaly (Chiang and Bitz 2005). The southward progress of negative water vapour anomalies is halted by an anomalous Hadley circulation associated with the southward shift of the Intertropical Convergence Zone that arises after the AMOC collapses (Vellinga and Wood 2002; Zhang and Delworth 2005; Chiang and Bitz 2005; Stouffer et al. 2006; Drijfhout 2010). Cvijanovic and Chiang (2013) and Liu et al. (2014) examined the radiative feedbacks associated with the response to North Atlantic cooling, using a radiative kernel analysis to quantify the various feedbacks on the top of the atmosphere (TOA) net flux. Both studies find that cloud shortwave and longwave water vapour to be important positive feedbacks that amplify the cooling in the NH, consistent with what is found here. There is a different cloud feedback in those studies and the albedo feedback from sea-ice is smaller. The different sea-ice response is obtained because these studies used a slab ocean model instead of the full dynamical model used here, and that, although the cloud response seems qualitatively similar in these models and for instance Zhang et al. (2010) and the present study, there are quantitative differences that may result from the strength of the cloud response in the tropics associated with a shift in the ITCZ and the opposing low and high cloud responses there versus the strength of the cloud response in the extratropics, especially in low clouds above the extratropical oceans.

After a century, the North Atlantic is much dryer and also the ice-cover anomaly has become much larger (Fig. 3e, f), but the anomalies do not cross the equator. Northward progressing positive water vapour anomalies are absent in the SH. Sea-ice changes are much smaller there, because the downwelling branch of the AMOC is narrow and concentrated in NH Deep Water formation sites near the ice edge, while the upwelling branch is broad and diffusive and spread around the SH (Winton 1995; Drijfhout et al. 2003). As a result, the water vapour response is weak in the SH (Fig. 2d). There, the temperature change closely follows the water vapour change that initially has the same sign as in the NH (Fig. 2c). In the first 30 years the SH even cools and after 100 years the SH warming is only 0.1 °C, while the NH cooling reaches 1.5 °C (Fig. 2a, c).

3.2 Formation of a halocline

Due to freshwater hosing a strong halocline forms in the subpolar North Atlantic and sea-surface salinities decrease.

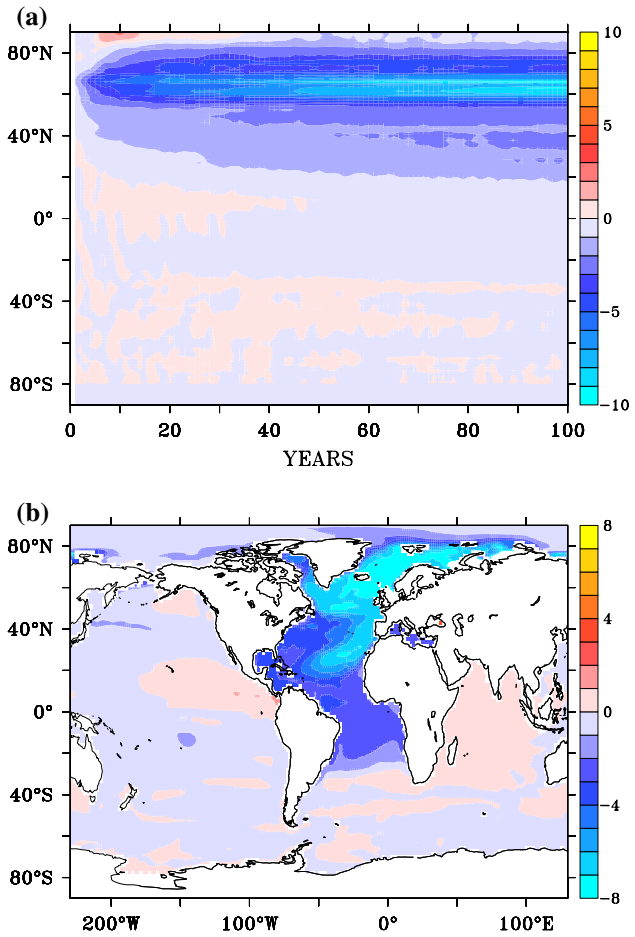

Fig. 4 **a** Zonally averaged sea surface salinity (SSS) as a function of time, being the difference in SSS between the two ensemble means. **b** Ten-year averaged pattern of SSS anomaly, being the difference in SSS between the two ensemble means between years 90–100

A possible explanation for the initial lack of warming in the SH could be that the amount of freshwater release is so large that this affects the SH as well and that the halocline in the SH reduces mixed-layer depths there, inhibiting an increase in heat uptake. Even with the unrealistically large amounts of freshwater hosing (1 Sv per year, mounting to 100 Sv years after a century), this forcing does not strongly affect SH surface salinities (Fig. 4a, b). The zonally averaged sea surface salinity anomaly does not progress southward of 20°N; in the SH only the South Atlantic is affected, but there is no signal in the Pacific and Indian Ocean, nor in the Southern Ocean (Fig. 4b).

3.3 The slow adjustment in ECHAM5 and SPEEDO

Although the sea-ice response is crucial for the fast, initial temperature response, the amplitude of the global cooling is determined by the water vapour feedback which eventually accounts for more than 80 % of the global cooling (Laurian

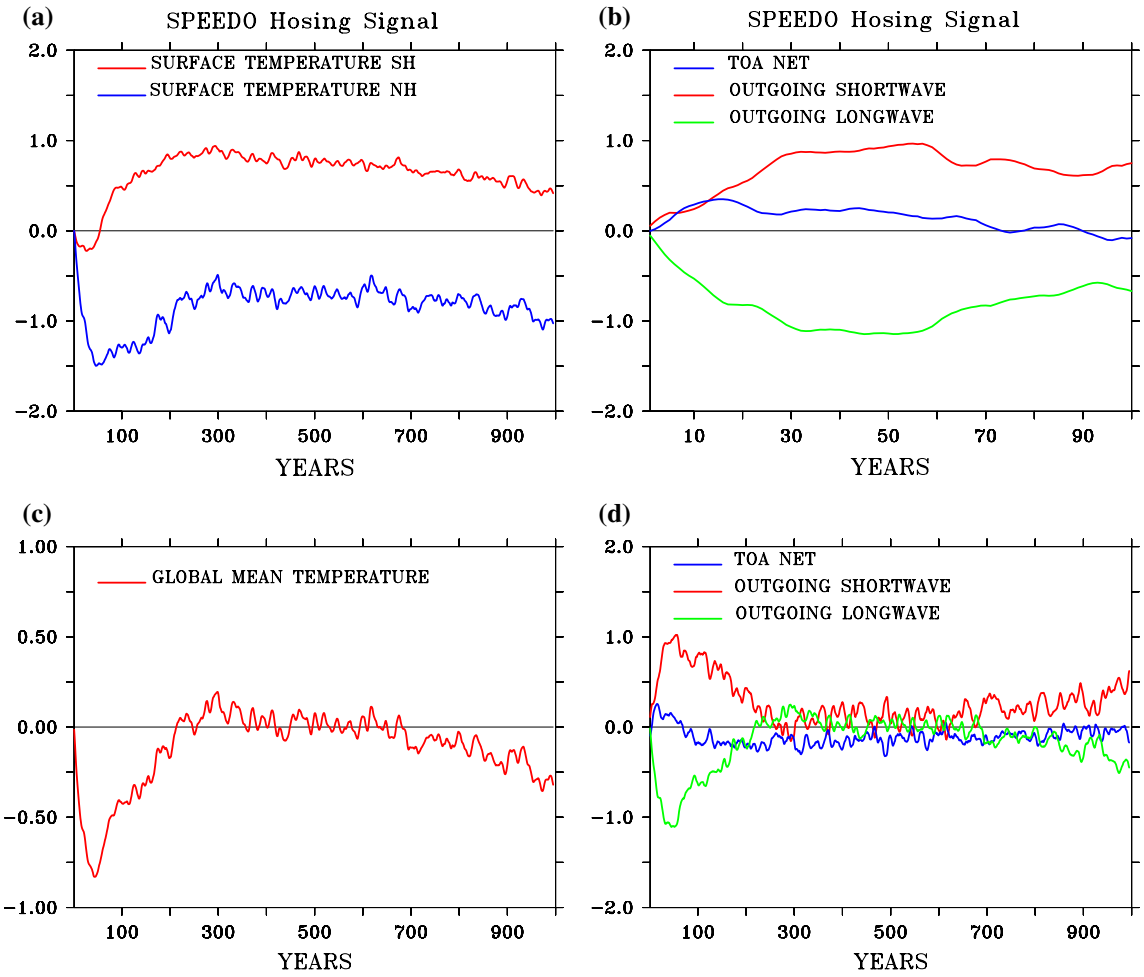

Fig. 5 **a** Northern and Southern Hemisphere global mean temperature anomalies in SPEEDO. All values have been smoothed with an 11-year low-pass filter and anomalies are defined relative to year 200 whereat freshwater hosing was applied for the first time. The time-series show years 200–1200. **b** Anomalies in globally averaged TOA radiation budget for SPEEDO during the first 100 years. **c** Thousand year evolution of GMT. **d** Same as **b**, but now for the whole 1,000-year period

et al. 2009). The fast feedbacks acting on the anti-symmetric heat transport forcing are very dissimilar in both hemispheres and the atmosphere on average cools. When the fast feedbacks have completed after 25 years, the response in the NH and SH slowly adjusts with warming in both hemispheres (Fig. 2e). A similar hosing experiment in a coupled model of intermediate complexity (SPEEDO; Cimatoribus et al. 2012a, b) shows that on longer timescales (100 years) the temperature response starts resembling a seesaw pattern (Fig. 5a). Associated with this adjustment, GMT increases after 25 years when SH warming starts to outpace NH cooling in the ECHAM5 model (Figs. 2e, 1b). In SPEEDO, the temperature increase occurs later; after 50 years.

The pattern of warming after the temperature minimum is reached in year 25 (Fig. 6a), shows warming over most of the NH and SH. Peaks in warming occur where the fast response is associated with peaks in cooling (Fig. 6b). Theses are the Labrador and Nordic Seas and the the northwest Pacific. Most regional differences are associated with changed winds. Hotspots of warming and ice melt occur where southerly winds develop in response to thermal high and low pressure fields (Zhang and Delworth 2005). Over the North Atlantic, North Pacific and Southern Ocean the surface cools where equatorward flow forces import of colder water from poleward areas. The thermal low over the North Pacific is particularly prominent and forces winds advecting air masses from the Arctic southward along the east coast of Siberia and Japan (Fig. 6c).

3.4 The radiation balance at TOA

The warming phase after the initial cooling is associated with a TOA radiation imbalance that results from the AMOC collapse because of net ocean heat uptake (Fig. 2f). Both increased sea-ice cover and decreased mixed-layer depths in the NH reduce the heat release from the ocean to

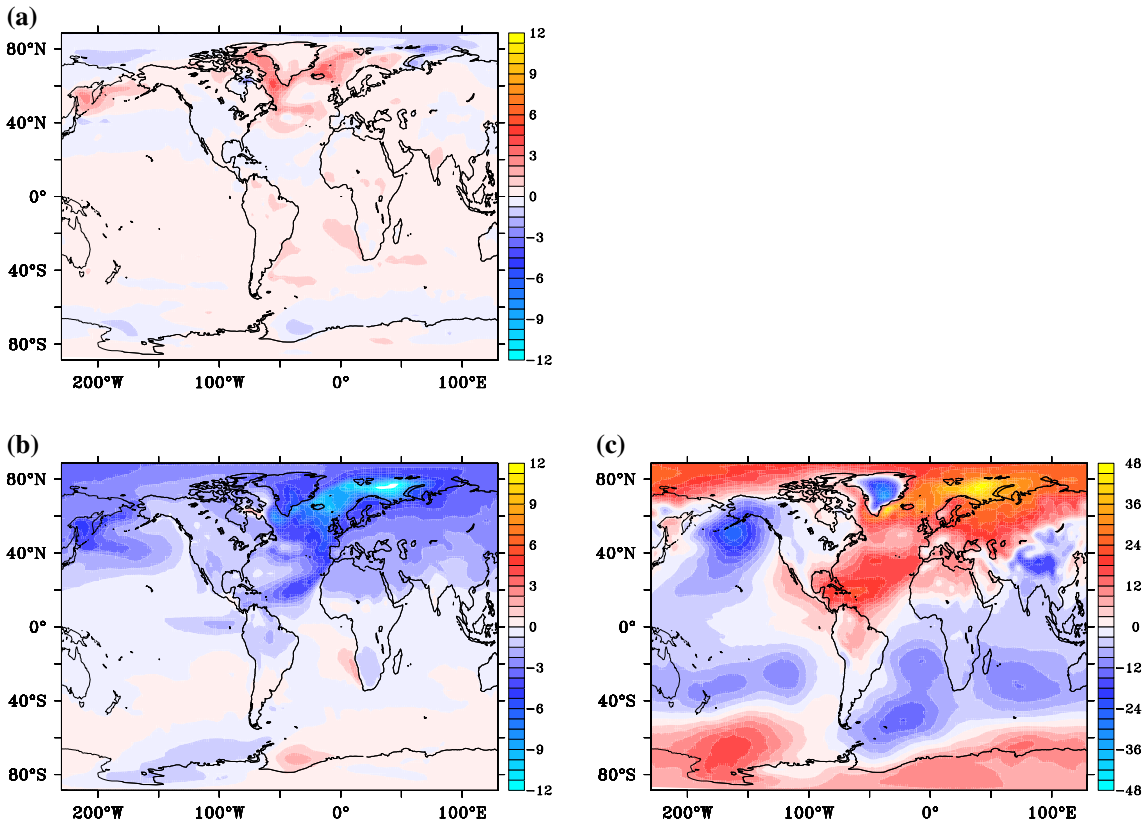

Fig. 6 **a** Temperature change associated with the slow feedback, being the difference in 10-year averaged temperature between the two ensemble means between years 90–100 and 20–30. **b** Temperature change associated with the fast feedback, being the difference in 10-year averaged temperature between the two ensemble means for years 20–30. **c** Sea level pressure anomaly associated with the fast feedback, being the 10-year averaged pressure difference between the two ensemble means for years 20–30

the atmosphere. The resulting heat uptake is accompanied by a comparably large TOA anomalous downward energy flow, because the heat capacity of the atmosphere is small. A downward TOA radiation anomaly and net ocean heat uptake are robust and model independent features that also arise for an AMOC collapse in a stationary climate simulation (Cheng et al. 2007; Vellinga and Wu 2008; Cimatoribus et al. 2012b), and in the hosing experiment with SPEEDO discussed here (Fig. 5b).

At first sight, the downward radiation anomaly at TOA may come as a surprise. Upward shortwave radiation at the surface increases with 0.82 W m^{-2} due to more sea-ice and snow cover. Reflection by clouds somewhat declines as cloud cover diminishes, but the TOA upward shortwave radiation anomaly is positive; 0.55 W m^{-2}. Net upward longwave radiation at the surface also increases. Trapping of longwave radiation near the surface is less efficient when the atmosphere becomes dryer, and this effect overcompensates reduced upward longwave radiation due to cooling of the surface. The rise in net upward longwave radiation is 0.71 W m^{-2}. Both changes conspire to create an outgoing radiation anomaly at TOA, but they are completely overruled by the change in longwave emission by the atmosphere. Longwave emission decreases with 1.95 W m^{-2}, resulting in a 0.69 W m^{-2} downward radiation anomaly at TOA, that after 25 years slowly diminishes with time (Fig. 2f). This decrease in atmospheric longwave emission almost exactly equals the decrease in turbulent heat flux from ocean to atmosphere (sensible and latent heat), implying energy conservation. Figure 2f underscores the tight relation between a radiation anomaly at TOA and ocean heat uptake.

The reduction in longwave emission by the atmosphere is nearly global (Fig. 7a). Increased emission occurs in the tropics where the Intertropical Convergence Zone and tropical clouds shifted southward (Chiang and Bitz 2005) and over the cold tongue in the North Atlantic where low clouds have formed (Laurian et al. 2010). In Laurian et al. (2010) it was shown that a strong secondary cloud response is set up with increased cloud cover over sea and decreased cloud cover over land. The cooler air temperature over the ocean in response to the collapse of the AMOC results in an increased stability of the atmospheric boundary layer, reducing entrainment of dryer air at the top of the marine

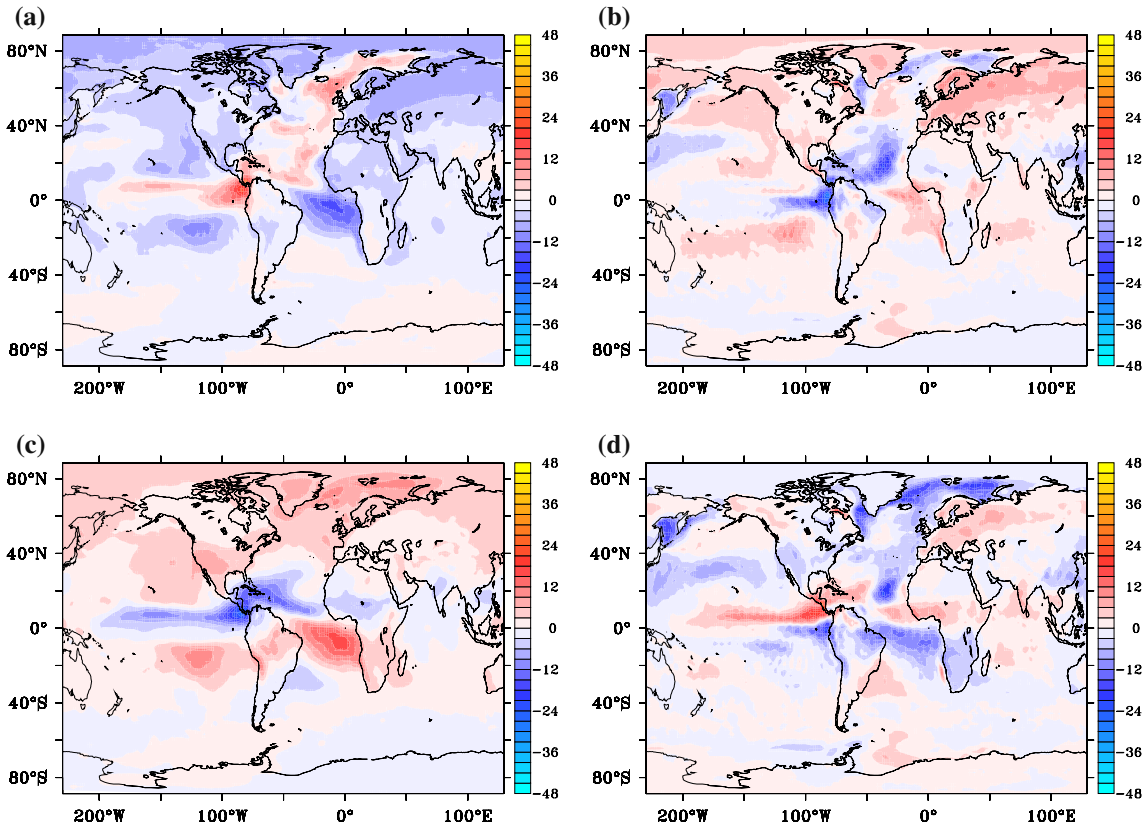

Fig. 7 **a** Ten-year averaged change in emitted longwave radiation by the atmosphere due to fast feedbacks for years 20–30 in W m^{-2}. **b** Same for the change in net downward radiation at TOA. **c** Same for the change in downward longwave radiation at TOA. **d** Same for the change in downward shortwave radiation at TOA

boundary layer. This leads to an increase of lower clouds over the ocean all year long, especially below 900 hPa. A similar increase in low clouds over the North Atlantic was found in Cvijanovic and Chiang (2013) after applying extratropical NH cooling.

The shifts in tropical low cloud and high cloud associated with the southward shift of ITCZ are opposite, i.e. low clouds shift northward, while high clouds shift southward with the ITCZ. They have completely different impact on the longwave and shortwave radiation (Zhang et al. 2010). Low clouds over the North Atlantic are visible in the net downward shortwave radiation at TOA (Fig. 7d), because they reflect more incoming shortwave radiation. The increase of low cloud over the North Atlantic will also reduce the net downward shortwave radiation at TOA, which amplifies the surface cooling in this region (Zhang et al. 2010). The North Atlantic is also the region where the net longwave flux at the surface has decreased, due to trapping by low clouds. As a result, the longwave is everywhere downward at TOA, apart from the northern tropics (Fig. 7c). The net downward TOA radiation (Fig. 7b) resembles the downward longwave signal, apart from some negative spots in the polar regions where pronounced increase in ice-cover induced larger upward shortwave fluxes.

This result reflects the dominant role of longwave radiation anomalies in establishing the TOA net radiation anomaly. In SPEEDO the net shortwave anomaly is larger than in ECHAM5, which results in a smaller TOA net radiation anomaly (Fig. 5b). In both ECHAM5 and SPEEDO the longwave and shortwave radiation anomalies at TOA decrease with time during the first 100 years (Figs. 2f, 5b). In ECHAM5, this results in slowly damping the GMT and TOA net radiation anomaly; after 100 years they have been reduced with 20 %. In SPEEDO, the decrease in TOA net radiation anomaly occurs faster and changes sign after 90 years. The GMT anomaly, as a result, is less quickly damped (Fig. 5c). The removal of the GMT anomaly occurs in about two centuries, but this does not result in the reestablishment of the initial equilibrium state. A period of 2–3 centuries follows in which the radiation anomalies at TOA are weak, and of opposite sign of the initial anomalies that established right after the AMOC collapse (Fig. 5d). The GMT-anomaly is slightly positive in this period. The apparent return to a state close to the initial climate, however, is hampered by the AMOC not recovering from the collapse.

Eventually, the TOA shortwave and longwave radiation anomalies grow again, regaining the same sign as during the first 25 years, when fast atmospheric feedbacks dominated the global response (Fig. 5d). The TOA net radiation anomaly remains small, but the ratio of outgoing shortwave to longwave radiation has changed, in line with a colder global mean surface temperature of 0.3 °C after 1,000 years (Fig. 5c). A comparison of Figs. 2 and 5 also reveals that the rise in GMT is accompanied by a decrease of TOA outgoing longwave and shortwave radiation anomalies. This change in GMT-trend occurs when SH warming starts and the change in TOA radiation anomalies after 25 years are dominated by the radiative adjustment in the SH.

4 Conclusions and discussion

Our main findings are that after a collapse of the AMOC fast atmospheric feedbacks induce an asymmetric response with NH cooling dominating SH warming, leading to a net GMT-anomaly. This anomaly is associated with net ocean heat uptake and TOA net downward radiation. After a few decades the planet warms and the GMT anomaly decreases. NH cooling and SH warming become more antisymmetric. This adjustment phase takes about 300 years. During these 300 years, the ocean heat content equilibrates with the circulation changes associated with the collapsed AMOC. SST changes are dominated by a seesaw pattern with Southern ocean warming and NH ocean basins cooling, most noticeably the North Atlantic. On even longer timescales, a slight recovery takes place in the Atlantic, with warming in the trade wind area according to a wind-evaporation-SST feedback (Xie and Philander 1994) and cooling along the Agulhas leakage path in the South Atlantic. In SPEEDO, Agulhas leakage occurs via a viscous boundary and after a shutdown of the AMOC, most Agulhas leakage continues to take place, but now feeding the subtropical gyre though the Brazil Current, instead of crossing the equator via the North Brazil Current (Laurian and Drijfhout 2011). On a millennium time scale SPEEDO simulates a gradual decrease of the Agulhas leakage in response to changing density and pressure differences between the Indian and South Atlantic Oceans. When ice-albedo feedbacks are stronger the TOA net radiation anomaly is smaller and damping of the GMT anomaly occurs slower. When the AMOC remains in the collapsed state an even slower radiative adjustment sets in after 300 years. Longwave and shortwave radiation anomalies at TOA increase again, associated with a cooling planet and GMT decreases. This radiative adjustment still has not reached equilibrium after 1,000 years of model integration. At these timescales CO_2 and ice-albedo feedbacks from large ice-sheets come into play, which may further modify the response to a collapse of the AMOC.

It cannot be inferred from these calculations how this scenario would be modified if the AMOC would recover during the first 1,000 years, although it seems likely that the slow radiative adjustment to a new equilibrium would have been absent in that case. It is intriguing that the initial shortwave adjustment in SPEEDO already is stronger than in ECHAM5. A larger TOA outgoing shortwave anomaly acts to reduce the TOA net downward radiation anomaly that initially arises when the AMOC collapses, associated with reduced ocean heat loss (net uptake). A larger shortwave response reduces radiative damping of the GMT anomaly that arises from fast atmospheric feedbacks and may promote adjustment to a colder climate. Experiments with different initial states in SPEEDO indicate that the larger shortwave response is not associated with cloud feedbacks, but is due to a larger (sea) ice-albedo response. This is facilitated by a colder pre-industrial climate (global mean SAT) in SPEEDO relative to the present-day climate in ECHAM5 (12.8 vs. 14.7 °C). So, the strength of the ice-albedo feedback, relative to other feedbacks associated with the longwave radiation response [greenhouse gas (water vapour) versus the Planck feedback] determines the radiative readjustment at TOA after an AMOC collapse. This is corroborated by the finding that during glacial times the recovery from an AMOC collapse develops slower than for pre-industrial times (Cheng et al. 2007; Weber and Drijfhout 2007).

Observations of past millennial changes in the Earths climate have indicated that slower climate feedbacks were linked to the ice-albedo feedbacks from changing large ice sheets, amplifying the initial response to changes in incoming solar radiation (Hansen et al. 2008). Another feedback that is not present in the models is the carbon feedback. In the past, transitions to colder conditions were accompanied by a lowering of atmospheric CO_2 (Alley et al. 2003; Hansen et al. 2008). The decline during abrupt transitions was estimated to be 10–40 ppm/1,000 years (Ahn and Brook 2008). This is not enough to counteract the radiative warming of 0.3 °C per century that occurs in the first centuries after an AMOC collapse (this number was estimated as the linear trend of the warming period between year 30 and 100 shown in Fig. 1a). However, in a colder and dryer climate, the net downward TOA anomaly after an AMOC collapse is smaller, since changes in atmospheric longwave emission will be less than changes in reflected shortwave radiation at the surface. The associated millennial-scale radiative adjustment to a new equilibrium is further modified by changes in CO_2 uptake by the oceans, or changes in CO_2 outgassing. How such an adjustment would be affected by a recovery or a more permanent shutdown of the AMOC remains to be answered by a fast, yet more complete Earth System Model than the models analysed here.

Acknowledgments The ESSENCE project, lead by Wilco Hazeleger and Henk Dijkstra, was carried out with support of DEISA, HLRS, SARA, and NCF (through NCF Projects NRG-2006.06, CAVE-60-023 and SG-06-267). The DEISA Consortium (co-funded by the EU FP6 Project 508830/031513) is thanked for support within the DEISA Extreme Computing Initiative. The author thanks Geert-Jan van Oldenborgh for suggestions and comments, Camiel Severijns for modelling support and two anonymous reviewers for their constructive criticism on an earlier version of the paper.

References

Alley RB et al (2003) Abrupt climate change. Science 299:2005–2010

Ahn J, Brook EJ (2008) Atmospheric CO_2 and climate on millennial time scales during the last glacial period. Science 322:83–85

Bjerknes J (1964) Atlantic air-sea interaction. Adv Geophys 10:1–82

Blunier T, Brook EJ (2001) Timing of millennial-scale climate change in Antarctica and Greenland during the last glacial period. Science 291:109–112

Broecker WS (1998) Paleocean circulation during the last deglaciation: a bipolar seesaw? Paleoceanography 13:119–121

Cheng W, Bitz CM, Chiang JCH (2007) Adjustment of the global climate to an abrupt slowdown of the Atlantic meridional overturning circulation. Ocean Circ Mech Impacts Geophys Monogr Ser 173:295–313

Chiang JCH, Bitz CM (2005) Influence of high latitude ice cover on the marine intertropical convergence zone. Clim Dyn 25:477–496

Cimatoribus AA, Drijfhout SS, Dijkstra HA (2012a) A global hybrid coupled model based on Atmosphere-SST feedbacks. Clim Dyn 38:745–760

Cimatoribus AA, Drijfhout SS, den Toom M, Dijkstra HA (2012b) Sensitivity of the Atlantic meridional overturning circulation to South Atlantic freshwater anomalies. Clim Dyn 39:2291–2306

Cvijanovic I, Chiang JCH (2013) Global energy budget changes to high latitude North Atlantic cooling and the tropical ITCZ response. Clim Dyn 40:1435–1452

Drijfhout SS (2010) The atmospheric response to a THC collapse: Scaling relations for the Hadley circulation and the nonlinear response in a coupled climate model. J Clim 23:757–774

Drijfhout SS, de Vries P, Döös K, Coward AC (2003) Impact of eddy-induced transport on the Lagrangian structure of the upper branch of the thermohaline circulation. J Phys Oceanogr 33:2141–2155

Drijfhout SS, Weber SL, van der Swaluw E (2011) The stability of the MOC as diagnosed from model projections for pre-industrial, present and future climates. Clim Dyn 37:1575–1586

Ganachaud A, Wunsch C (2003) Large-scale ocean heat and freshwater transports during the World Ocean Circulation Experiment. J Clim 16:696–705

Hansen J et al (2008) Target atmospheric CO_2: where should humanity aim? The Open Atmos Sci J 2:213–217

Jackson LC (2013) Shutdown and recovery of the AMOC in a coupled global climate model: the role of the advective feedback. Geophys Res Lett 40:1182–1188

Laurian A, Drijfhout SS, Hazeleger W, van Dorland R (2009) Global surface cooling: the atmospheric fast feedback response to a collapse of the thermohaline circulation. Geophys Res Lett. doi:10.1029/2009GL040938

Laurian A, Drijfhout SS, Hazeleger W, van den Hurk B (2010) Response of the Western European climate to a collapse of the thermohaline circulation. Clim Dyn 34:689–697

Laurian A, Drijfhout SS (2011) Response of the South Atlantic circulation to an abrupt collapse of the Atlantic meridional overturning circulation. Clim Dyn 37:521–530

Liu Y, Chiang JCH, Chou C, Patricola CM (2014) Atmospheric teleconnection mechanisms of extratropical North Atlantic SST influence on Sahel rainfall. Clim Dyn. doi:10.1007/s00382-014-2094-8

Marsland SJ, Haak H, Jungclaus JH, Latif M, Röske F (2003) The Max-Planck-Institute global ocean/sea ice model with orthogonal curvilinear coordinates. Ocean Modell 5:91–127

Roeckner E et al. (2003) The atmospheric general circulation model ECHAM 5. Part I: Model description. Max-Planck-Institute Report 349, 127 pp

Severijns CA, Hazeleger W (2009) The efficient global primitive equation climate model SPEEDO. Geosci Model Dev Discuss 2:11–15

Stocker TF, Johnsen SF (2003) A minimum thermodynamic model for the bipolar seesaw. Paleoceanography. doi:10.1029/2003/PA000920

Stouffer RJ et al (2006) Investigating the causes of the response of the thermohaline circulation to past and future climate changes. J Clim 19:1365–1387

Trenberth KE, Fasullo JT, Kiehl J (2009) Earth's global energy budget. Bull Am Meteorol Soc 90:311–324

Vellinga M, Wood RA (2002) Global climatic impacts of a collapse of the Atlantic thermohaline circulation. Clim Change 54:251–267

Vellinga M, Wu P (2008) Relations between northward ocean and atmosphere energy transports in a coupled climate model. J Clim 21:561–575

Weber SL, Drijfhout SS (2007) Stability of the Atlantic meridional overturning circulation in the Last Glacial Maximum climate. Geophys Res Lett. 34 doi:10.1029/2007GL031437

Winton M (1995) Why is the deep sinking narrow? J Phys Oceanogr 25:997–1005

Xie S-P, Philander SGH (1994) A coupled ocean-atmosphere model of relevance to the ITCZ in the eastern Pacific. Tellus 46A:340–350

Zhang R, Delworth TL (2005) Simulated tropical response to a substantial weakening of the Atlantic thermohaline circulation. J Clim 18:1853–1860

Zhang R, Kang SM, Held IM (2010) Sensitivity of climate change induced by the weakening of the Atlantic meridional overturning circulation to cloud feedback. J Clim 23:378–389